Dalton Transactions

ARTICLE

Improving the SMM and luminescent properties of lanthanide complexes with LnO_9 cores in the presence of Zn^{II}: an emissive Zn_2Dy single ion magnet

Received 00th January 20xx,
Accepted 00th January 20xx

DOI: 10.1039/x0xx00000x

www.rsc.org/

Matilde Fondo,[a,*] Julio Corredoira-Vázquez,[a] Antía Herrera-Lanzós,[a] Ana M. García-Deibe,[a] Jesús Sanmartín-Matalobos,[a] Juan Manuel Herrera,[b] Enrique Colacio,[b] and Cristina Nuñez[a,c]

Mononuclear complexes of stoichiometry $[Ln(H_3L)(H_2O)(NO_3)](NO_3)_2$ (Ln = Tb, **1**; Dy, **2**, Er, **3**), which crystallise with different solvates, and the heterotrinuclear compound $[Zn_2Dy(L)(NO_3)_3(OH)]$ (**4**) can be obtained with the same H_3L compartmental ligand. The single X-ray crystal structure of the mononuclear complexes shows a LnO_9 core with a muffin-like disposition while the geometry of the DyO_9 core in **4** seems to be closer to spherical capped square antiprism. The analysis of the magnetic properties of all the complexes demonstrates that the mononuclear lanthanide compounds do not show slow relaxation of the magnetization, even when the samples are diluted with a diamagnetic matrix and subjected to the presence of a *dc* applied field of 1000 Oe. Nevertheless, the heterotrinuclear dysprosium complex **4**·$3H_2O$ is a field-induced single ion magnet, with an estimated U_{eff} barrier of 59 K. The luminescent characterisation of all the metal complexes in methanol solution at 298 K also shows a notable increase in the fluorescent emission of the heterotrinuclear complex respect to the mononuclear ones, in such a way that **4** can be defined as a fluorescent single ion magnet.

Introduction

Multifunctional materials combining different physical properties is a hot research topic in chemistry of materials.[1] In this way, the concurrence of magnetic and emission effects is particularly promising as it not only can lead to bifunctional materials but also opens the possibility of tuning light emission by a magnetic field.[2,3] The studies on this particular field were initially focused on emissive ferromagnets, due to their applications in optoelectronics and multimodal sensing. These substances are based on nanocomposites of fluorescent quantum dots, organic dyes, or f-metal complexes, bounded with magnetic nanoparticles.[4] Nevertheless, the area of the emissive magnetic materials is not restricted to this kind of product and, more recently, luminescent molecular magnets have appeared as a novel and exciting idea.[5] However, a rational synthetic design is mandatory to achieve relevant magnetic and luminescent properties in metal complexes. In this sense, the use of lanthanides seems to have some advantages, both inducing SMM and emissive behaviour.

The luminescent emission in lanthanide complexes is usually enhanced by the use of appropriate light-harvesting units such as organic ligands[6] or metal complexes based on d-metal ions (e.g., Zn(II) and Ir(III))[7-8] or, less frequently, alkaline earth metals (such as Mg(II)).[8] The use of Zn(II) is particularly interesting because of some peculiar characteristics of this metal ion. First, Zn(II) is diamagnetic and thus any intramolecular magnetic interaction with the lanthanide centres is avoided. This is generally appreciated because although the merging of 3d-4f spin carriers can be an effectively way of suppressing the zero-field quantum tunnelling mechanism,[9-11] weak magnetic interactions can also promote fast relaxation of the magnetization and damp the SMM behaviour.[12-13] Second, it has been demonstrated both theoretically and experimentally that the introduction of Zn(II) usually increases the energy anisotropic barrier.[8,14-17]

Besides, Zn^{2+} can be encapsulated in small ligands and has a preference for low coordination numbers (4-6) while lanthanide ions are more bulky and tend to achieve higher coordination numbers (usually higher than 8). These differences in size and coordination preferences allow to predesign ligands that can allocate both kinds of metal ions in predetermined pockets.

With these considerations in mind, the old ligand H_3L (Scheme 1) previously reported by us[18] was revised under the light of its compartmental character, with pockets of different size. The reactivity of this ligand towards Ln(III) ions (Ln = Tb, Dy, Er) and towards Ln(III) and Zn(II) ions was studied. The results achieved, which include the study and comparison of the magnetic and luminescent properties of the isolated complexes, are described herein.

[a] Departamento de Química Inorgánica, Facultade de Química, Universidade de Santiago de Compostela, 15782 Santiago de Compostela, Spain
E-mail: matilde.fondo@usc.es.
[b] Departamento de Química Inorgánica, Facultad de Ciencias, Universidad de Granada, Avda. Fuentenueva s/n, 18071, Granada (Spain).
[c] Oncology Division, Research Unit, Hospital Universitario Lucus Augusti (HULA), Servizo Galego de Saúde (SERGAS), 27002 Lugo, Spain

Electronic Supplementary Information (ESI) available: Tables S1-S3 and Figures S1-S6. CCDC 1574339 (**1**·CH_3CN), 1574341 (**2**·$0.5CH_3CN$), 1574342 (**3**) and 1574343 (**4**·$(CH_3)_2CO$). For ESI and crystallographic data in CIF format see DOI: 10.1039/x0xx00000x.

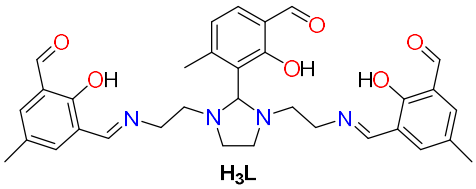

H_3L

Scheme 1

Experimental

Materials and general methods

All chemical reagents and solvents were purchased from commercial sources and used as received without further purification. Elemental analyses of C, H and N were performed on a Carlo Erba EA 1108 analyser. Infrared spectra were recorded in the ATR mode on a Varian 670 FT/IR spectrophotometer in the range 4000-500 cm^{-1}.

Syntheses of the complexes

All the mononuclear complexes were obtained by template synthesis, in a similar way that will be exemplified by the synthesis of $[Tb(H_3L)(H_2O)(NO_3)](NO_3)_2$ (**1**): to a solution of triethylenetetramine (0.038 g, 0.26 mmol) in methanol (20 mL), 2-hydroxy-5-methyl-1,3-benzenedicarboxaldehyde (0.13 g, 0.79 mmol) and acetonitrile (10 mL) were added. The mixture was stirred for 30 min and $Tb(NO_3)_3{\cdot}5H_2O$ (0.114 g, 0.26 mmol) was added to the obtained yellow solution. The new mixture was stirred for 16 h at room temperature and the resultant yellow solution was concentrated in a rotaevaporator, reducing its volume up to 15 mL. The solution was left to refrigerate in the fridge and after 24 h, single crystals of **1**·CH_3CN, suitable for X-ray diffraction studies, precipitated. The crystals were filtered and dried in air, losing the acetonitrile solvate to give rise to **1**. Yield: 0.15 (61%). M.W.: 947.67. Anal. calcd. for $C_{33}H_{38}TbN_7O_{16}$: C 41.79, H 4.00, N 10.34 %. Found: C 41.57, H 4.32, N 10.49 %. IR (ATR, $\tilde{\nu}/cm^{-1}$): 3260 (H_2O), 1647 (C=O), 1631 (C=N), 1276, 1300 (NO_3^-).

$[Dy(H_3L)(H_2O)(NO_3)](NO_3)_2$ (**2**): quantity of $Dy(NO_3)_3{\cdot}xH_2O$: 0.091 g (0.26 mmol). Single crystals of **2**·0.5CH_3CN are isolated in the same way as those of **1**·CH_3CN, which lose the acetonitrile solvate on drying to yield **2**. Yield: 0.11 g (44%). M.W.: 951.10. Anal. calcd. for $C_{33}H_{38}DyN_7O_{16}$: C 41.67, H 4.03, N 10.31 %. Found: C 41.57, H 4.32, N 10.49 %. IR (ATR, $\tilde{\nu}/cm^{-1}$): 3266 (H_2O), 1646 (C=O), 1635 (C=N), 1283, 1303 (NO_3^-).

$[Er(H_3L)(H_2O)(NO_3)](NO_3)_2$ (**3**): quantity of $Er(NO_3)_3{\cdot}5H_2O$: 0.115 g (0.26 mmol). Single crystals of **3** are isolated in the same way as those of **1**·CH_3CN. Yield: 0.12 (48%). M.W.: 955.96. Anal. calcd. for $C_{33}H_{38}ErN_7O_{16}$: C 41.42, H 3.97, N 10.25 %. Found: C 41.44, H 4.04, N 9.85 %; IR (ATR, $\tilde{\nu}/cm^{-1}$): 3330 (H_2O), 1644 (C=O), 1634 (C=N), 1285, 1302 (NO_3^-).

$[Dy_{0.09}Y_{0.91}(H_3L)(H_2O)(NO_3)](NO_3)_2$ (**2@Y**): A sample of **2** diluted with yttrium was prepared by mixing **2** and $[Y(H_3L)(H_2O)(NO_3)](NO_3)_2$ in 1:10 molar ratio. $[Y(H_3L)(H_2O)(NO_3)](NO_3)_2$ was obtained in exactly the same way as **2**: quantity of $Y(NO_3)_3{\cdot}6H_2O$: 0.099 (0.26 mmol). Yield: 0.15 g (66%). M.W.: 877.56. Anal. calcd. for $C_{33}H_{38}YN_7O_{16}$: C 45.13, H 4.33, N 11.07 %. Found: C 45.14, H 4.51, N 10.94 %. IR (ATR, $\tilde{\nu}/cm^{-1}$): 3262 (H_2O), 1645 (C=O), 1633 (C=N), 1284, 1305 (NO_3^-).

$[Zn_2Dy(L)(NO_3)_3(OH)]\cdot$ (**4**): to a solution of triethylenetetramine (0.038 g, 0.26 mmol) in methanol (20 mL), 2-hydroxy-5-methyl-1,3-benzenedicarboxaldehyde (0.13 g, 0.79 mmol) and acetonitrile (10 mL) were added. The mixture was stirred for 30 min and $Zn(OAc)_2{\cdot}2H_2O$ (0.128 g, 0.52 mmol) was added to the obtained yellow solution. The new mixture was stirred for 10 min and then $Dy(NO_3)_3{\cdot}xH_2O$ (0.091 g, 0.26 mmol) was added to the new yellow solution. The new mixture was stirred at room temperature for 4 h and the resultant solution was concentrated in a rotaevaporator, reducing its volume up to 15 mL. The solution was left to refrigerate in the fridge and after 4 days a powder solid precipitates. The solid was filtered and dried in an oven for 4 h at 80 ºC. Yield: 0.10 g (36%). M.W.: 1077.91. Anal. calcd. for $C_{33}H_{34}DyN_7O_{16}Zn_2$: C 36.74, H 3.15, N, 9.09 . Found: C 36.65, H 3.35, N 9.15 %. IR (ATR, $\tilde{\nu}/cm^{-1}$): 3391 (OH), 1647 (C=O), 1631 (C=N), 1306 (NO_3^-).

Recrystallization of the powder solid, by diffusion of diethyl ether into a methanol/acetone solution of **4** with a few drops of cyclohexane, yields single crystals of **4**·$(CH_3)_2CO$, suitable for X-ray diffraction studies.

Crystallographic refinement and structure solution

Crystal data and details of refinement are given in Table S1. Single crystals of **1**·CH_3CN, **2**·0.5CH_3CN, **3** and **4**·$(CH_3)_2CO$ were obtained as detailed above. Data were collected at 100 K on a Bruker Kappa APEXII CCD diffractometer, employing graphite monochromated Mo-kα (λ = 0.71073 Å) radiation. Multi-scan absorption corrections were applied using SADABS.[19] The structures were solved by standard direct methods, and then refined by full-matrix least-squares techniques on F^2, using the program package SHELX.[20] All non-hydrogen atoms were refined anisotropically, with some exceptions, corresponding to disordered solvates with low occupation sites. The hydrogen atoms were mostly included in the structure factor calculations in geometrically idealized positions. However, some of the H atoms attached to oxygen and/or nitrogen atoms were located in the Fourier map, with the intention of detecting H bonding schemes.

Magnetic measurements

Magnetic susceptibility measurements for powder crystalline samples of **1**, **2**, **3** and **4** were carried out with a Quantum Design SQUID MPMS-XL-5 susceptometer. The magnetic susceptibility data were recorded under magnetic fields of 1000 Oe in the range 2-300 K. Magnetization measurements at 2.0 K were recorded under magnetic fields ranging from 0 to 50000 Oe. Diamagnetic corrections were estimated from Pascal's Tables. *ac* susceptibility measurements in different applied static fields (H_{dc} = 0, 1000 or 2500 Oe) were performed with an oscillating *ac* field of 3.5 Oe and *ac* frequency of 1200 Hz for all the complexes with a Quantum Design SQUID MPMS XL-5 device. For **2@Y** the measurements were recorded at 1400 Hz. In the case of **4**, *ac* susceptibility measurements were also recorded in a *dc* field of 2500 Oe at *ac* frequencies ranging from 50 to 1400 Hz.

Spectrophotometric and spectrofluorimetric measurements

Absorption spectra were recorded on a JASCO V-630 spectrophotometer and fluorescence emission spectra on a JASCO FP-8300 spectrofluorimeter. The linearity of the fluorescence emission versus concentration was checked in the concentration range used (10^{-4}-10^{-6} M). The correction of the absorbed light was performed when considered necessary.

The spectrophotometric characterisation was made by preparing stock solutions of **1**, **2**, **3** and **4** in methanol (*ca.* 10^{-3} M). The studied solutions were prepared by appropriate dilution of the stock solutions up to 10^{-5}-10^{-6} M. Fluorescence quantum yields were determined using a 0.1 M solution of quinine sulphate in 0.5 M H_2SO_4 as standard ($\phi = 0.546$) and all values were corrected taking into account the solvent refraction index.[21] All the measurements were taken at 298 K.

Results and discussion

Mononuclear Tb^{III}, Dy^{III} and Er^{III} complexes were obtained by template synthesis, as summarised in Scheme 2. The mixing of all components in appropriate molar ratios give solutions that, on cooling on the fridge, yield single crystal of $[Tb(H_3L)(NO_3)(H_2O)](NO_3)_2{\cdot}CH_3CN$ (**1**·CH_3CN), $[Dy(H_3L)(NO_3)(H_2O)](NO_3)_2{\cdot}0.5CH_3CN$ (**2**·$0.5CH_3CN$) and $[Er(H_3L)(NO_3)(H_2O)](NO_3)_2$ (**3**). Drying of the single crystals lead to loss of all solvates for the Tb and Dy compounds. Accordingly, the final products are **1**, **2** and **3**.

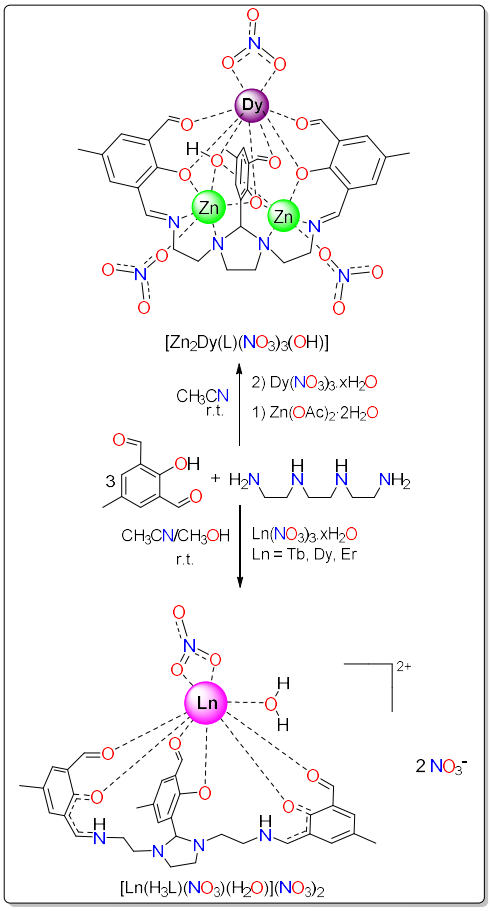

Scheme 2

The isolation of these mononuclear complexes is rather unexpected, as it is well known that this kind of acyclic compartmental Schiff base derived from triethylenetetramine and aromatic aldehydes usually yields dinuclear lanthanide complexes of formula $[Ln(L)]_2$, with a sandwich structure.[22-26] The crystallographically characterised reported exceptions to this rule are one praseodymium and one neodymium complex,[27] both obtained as by-products from the hydrolysis of related compounds. Therefore, complexes **1**, **2** and **3** are, as far as we know, the first mononuclear lanthanide complexes containing an api-type ligand (H_3api = 2-(2-hydroxyphenyl)-1,3-bis[4-(2-hydroxyphenyl)-3-azabut-3-enyl]-1,3-imidazolidine) obtained as main products of a systematic reaction approach, and fully characterised.

The heterotrinuclear complex $[Zn_2DyL(NO_3)_3(OH)]$ (**4**) could be also obtained by template synthesis, by mixing the dialdehyde, the tetramine, $Zn(OAc)_2{\cdot}2H_2O$ and $Dy(NO_3)_3{\cdot}xH_2O$ in 3:1:2:1 molar ratios (Scheme 2). Single crystals of **4** could be isolated by diffusion of diethyl ether into a methanol/acetonitrile solution of the powder sample, containing a few drops of cyclohexane. Nevertheless, in spite of the multiple attempts, no similar Zn_2Tb or Zn_2Er complexes could be obtained and unequivocally characterised.

All these compounds are yellow solids, apparently stable in solid state and in solution, and their formulations were confirmed by microanalysis, IR spectroscopy and by single X-ray diffraction studies. Their magnetic behaviour and luminescence properties were also analysed.

The infrared spectra of all the compounds contain a sharp band at *ca*. 1645 cm^{-1}, assigned to $\nu(C{=}O)_{aldehyde}$. When the aldehyde group of this ligand remains uncoordinated, as in the previously reported $[Zn_2L(OAc)]$ complex,[18] it gives rise to an IR band at 1673 cm^{-1}. The displacement of this band about 30 cm^{-1} in **1**, **2**, **3** and **4** respect to $[Zn_2L(OAc)]$ suggests the involvement of the $O_{aldehyde}$ atom in the coordination to the metal ions. In addition, a second sharp band, which partially overlaps with that of the carbonyl group, can be observed at *ca.* 1635 cm^{-1}, in agreement with the presence of the imine moiety in the molecules.[18,28] Besides, all the mononuclear complexes show two sharp bands at *ca.* 1300 and 1280 cm^{-1}, assigned to N-O vibrations of nitrate.[28] The presence of two strong bands in this region of the spectra agrees with two different modes of actuation of the nitrate group.[28] In the case of **4**, these two bands appear as a quite broad intense band at 1306 cm^{-1}, also corroborating the presence of the nitrate groups in the complex. Finally, all the spectra also show a band centred at *ca*. 3300 cm^{-1}, indicating the presence of coordinated water or hydroxide.[28]

X-ray diffraction studies

Mononuclear complexes

The crystal structures of $[Tb(H_3L)(NO_3)(H_2O)](NO_3)_2{\cdot}CH_3CN$ (**1**·CH_3CN), $[Dy(H_3L)(NO_3)(H_2O)](NO_3)_2{\cdot}0.5CH_3CN$ (**2**·$0.5CH_3CN$) and $[Er(H_3L)(NO_3)(H_2O)](NO_3)_2$ (**3**) are very similar. The main difference among them is that **1** and **3** has a symmetry plane (space group $P2_1/m$), which contains the metal ion and the central phenol ring, thus making crystallographically equivalent both halves of the molecules. This plane does not exist in **2** (space group $P2_1$). Despite this, given the high structural similarity, the structures of all the complexes will be discussed together.

Figures S1, 1 and 2 show ellipsoid diagrams for **1**, **2** and **3**, respectively, and selected bond distances and angles for the three compounds are recorded in Table 1.

In all the complexes, the unit cell contains $[M(H_3L)(H_2O)(NO_3)]^{2+}$ cations, two nitrate anions per cation and acetonitrile as solvate in the case of the Tb and Dy compounds. In the cation, the Schiff base is not deprotonated and the hydrogen atoms linked to heteroatoms were found in the Fourier map nearer to the N_{imine} atoms than to O_{phenol} ones, which seems to indicate that the keto-amine form of the ligand is more stable than the phenol-imine one.

In all cases H_3L acts as hexadentate, using all its oxygen atoms (three O_{phenol} and three $O_{aldehyde}$) to bind the Ln^{3+} ion, with all the nitrogen atoms remaining uncoordinated. The coordination spheres of the lanthanide ions are completed by a nitrate ligand, acting as bidentate chelate, and a water molecule. Accordingly, the Ln^{3+} ions reach a coordination number of 9. The distortions from the ideal nine-coordinate geometries for the LnO_9 cores were computed using SHAPE software[29] and the less deviation has been found for a muffin-like structure (Table S2), as shown in Fig. 3.

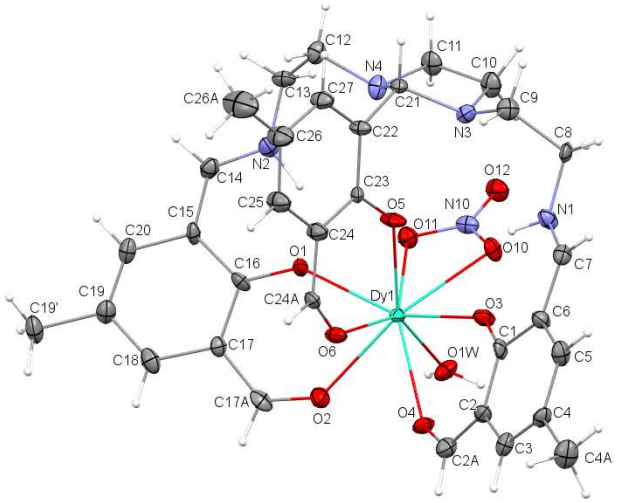

Fig. 1. Ellipsoid (50% probability) diagram for the cation $[Dy(H_3L)(H_2O)(NO_3)]^{2+}$ in **2**.

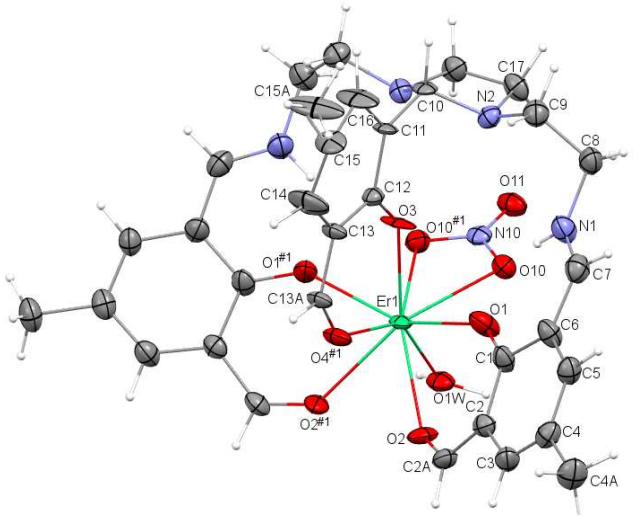

Fig. 2. Ellipsoid (50% probability) diagram for the cation $[Er(H_3L)(H_2O)(NO_3)]^{2+}$ in **3**.

Table 1. Main bond distances (Å) and angles (º) for **1**·CH_3CN, **2**·0.5CH_3CN and **3**

	1·CH_3CN	**3**	**2**·0.5CH_3CN	
M1—O1	2.357(2)	2.314(7)	Dy1—O1	2.350(6)
			Dy1—O3	2.346(6)
M1—O2	2.479(2)	2.460(7)	Dy1—O2	2.452(7)
			Dy1—O4	2.485(7)
M1—O3	2.306(3)	2.266(10)	Dy1—O5	2.299(4)
M1—O4	2.380(3)	2.334(10)	Dy1—O6	2.363(3)
M1—O10	2.527(2)	2.496(7)	Dy1—O10	2.520(8)
			Dy1—O11	2.503(8)
M1—O1W	2.391(3)	2.351(9)	Dy1—O1W	2.378(3)
O1-M-O1$^{\#1}$	147.07(15)	146.7(5)	O1-Dy-O3	147.5(2)
O10-M-O10$^{\#1}$	50.55(10)	50.8(3)	O10-Dy-O11	50.77(13)

$^{\#1}$ *x*, -*y*+1/2, *z*

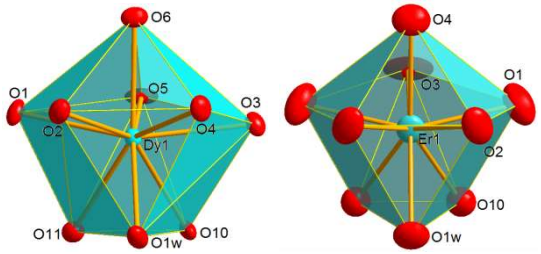

Fig. 3. Coordination environments for the Ln ion in **2** and **3**, showing the muffin-like structure. The environment for Tb in **1** is very similar.

In all these structures the M-O distances range from 2.26 to 2.53 Å, and they are comparable with those previously reported for lanthanide complexes with O-donor ligands.[30-31] The shortest M-O distance corresponds to the bond between the metal ion and the oxygen atom of the central phenolic ring (O3 for **1** and **3**, and O5 for **2**) and the longest M-O distances correspond to the bonds between the metal centre and the nitrate ligand. The angles about the lanthanide ion vary from 50 to 148 º and they are also in their usual range.[30-31]

Finally, note that the structures of all the complexes are further stabilised by hydrogen bonds. Thus, the $[M(H_3L)(H_2O)(NO_3)]^{2+}$ cations show intramolecular interactions between the phenolic oxygen atoms and the nitrogen atoms of the chain. In addition, hydrogen bonds are also observed between the coordinated water molecule and the nitrate counterions, as it is exemplified for **2** in Fig. 4.

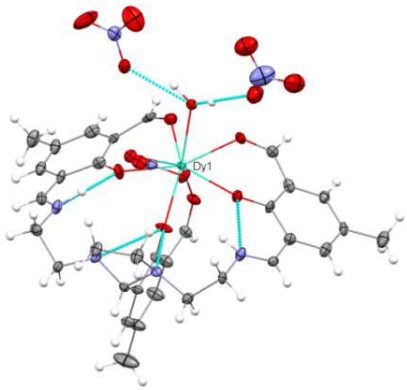

Fig. 4. Ellipsoid (50% probability) diagram for **2**, showing the hydrogen bond scheme.

$[Zn_2DyL(NO_3)_3(OH)]\cdot(CH_3)_2CO$ ($4\cdot(CH_3)_2CO$)

The crystal structure shows that·**4**·$(CH_3)_2CO$ consists of trinuclear $[Zn_2DyL(NO_3)_3(OH)]$ (**4**) units (Figure 5) with acetone as solvate. The structure of **4** has a symmetry plane that contains the dysprosium ion and the central phenol ring, and that bisects the nitrate ligand, thus making both halves of the molecule crystallographically equivalent.

4 can be understood as a $[Zn_2L(NO_3)_2(OH)]^{2-}$ fragment that acts as a metalloligand towards a Dy^{3+} ion. Thus, in this fragment, the Schiff base, which is fully deprotonated, allocates a zinc(II) ion in each one of its internal N_2O compartments (O1N1N2). In addition, both zinc centres are bridged by an endogenous phenolate oxygen atom (O3) of the central ligand arm, the carbonyl oxygen atoms remaining uncoordinated. The coordination spheres of the zinc centres are completed by two nitrate anions, coordinated each one to a Zn^{II} ion as a monodentate terminal donor, and by a hydroxide ligand, acting as a bridge between the zinc atoms. This gives rise to a coordination number of 6 for the zinc atoms, with distorted octahedral geometry.

The above described $[Zn_2L(NO_3)_2(OH)]^{2-}$ anion joins a Dy^{3+} ion, using all of its carbonyl and phenolic oxygen atoms (a total of 6) to link to the lanthanide metal, as in the mononuclear complexes. In addition, the hydroxide ligand also binds the dysprosium atom, acting now as a μ_3 bridge.

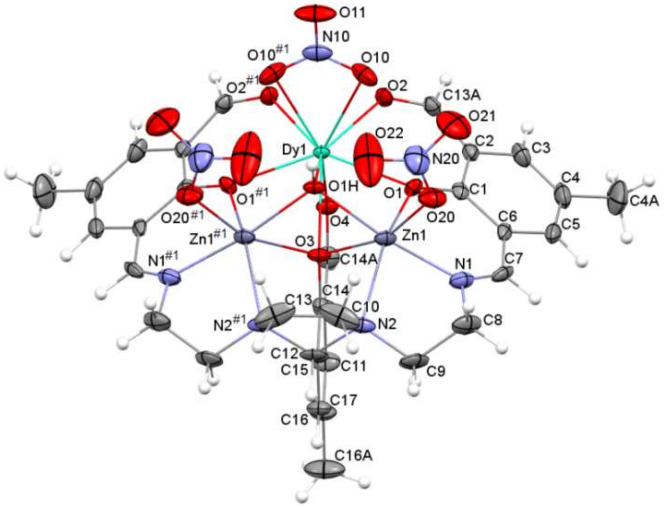

Fig. 5. Ellipsoid (50% probability) diagram for **4**.

Table 3. Main bond distances (Å) and angles (º) for **4**·$(CH_3)_2CO$

Dy1-O1	2.312(3)	Zn1-N1	2.034(5)
Dy1-O2	2.360(3)	Zn1-O1H	2.048(3)
Dy1-O1H	2.362(5)	Zn1-O20	2.103(4)
Dy1-O4	2.411(5)	Zn1-O1	2.154(3)
Dy1-O3	2.439(5)	Zn1-O3	2.219(3)
Dy1-O10	2.485(4)	Zn1-N2	2.234(4)
Dy1···Zn1	3.2000(7)	Zn1···$Zn1^{\#1}$	3.288(1)
$O10^{\#1}$-Dy1-O10	51.1(2)	Zn1-O1H-Dy1	92.71(17)
O4-Dy1-N10	159.1(18)	Zn1-O1-Dy1	91.47(13)
N1-Zn1-O1H	172.98(18)	Zn1-O3-Dy1	86.66(14)
O20-Zn1-O3	161.05(16)	Zn1-O3-$Zn1^{\#1}$	95.59(18)
		Zn1-O1H-$Zn1^{\#1}$	106.8(2)

$^{\#1}$ x, -y+1/2, z

The coordination sphere of the lanthanide centre is completed by a bidentate chelate nitrate, thus giving rise to a DyO_9 environment, as in **2**, where the only difference in the donor atoms about the Dy ion is that the water molecule in the coordination sphere in **2** was replaced by a hydroxide ligand in **4**. Computations with the SHAPE software[29] indicate that the geometry about the Dy^{3+} ion is now closest to spherical capped square antiprism (Table S2, Fig. 6), but with a significant distortion towards muffin-like. This implies a small change in the environment of the dysprosium ion in **4** with respect to **2** but, once again, all the bond distances and bond angles in **4** are in the usual range,[30-31] and do not merit further consideration.

It should be noted that this structure is remarkably different from the one described for $[Zn_2Dy(L')(OAc)_2(NO_3)_2(H_2O)]$,[30] where the main difference between L and L′ is that the carbonyl group in L (3-position on the aromatic ring) has been replaced by a methoxy donor in L′. The comparison of both crystal structures clearly shows that the substitution of methoxy groups by carbonyl ones increases the ability of the group at the 3-position on the aromatic ring to act as a donor, and therefore, the denticity of the ligand. Thus, the denticity of L' in $[Zn_2Dy(L')(OAc)_2(NO_3)_2(H_2O)]$ is 8, with the methoxy groups of two ligand arms remaining uncoordinated, while the denticity of L in **4** is 10, using all its potential donor atoms. Accordingly, this comparison demonstrates that small changes in the nature of the aromatic ring substituents can give rise to important differences in the coordination mode of this kind of ligand.

Finally, it is worth of mention that the zinc atoms in **4** are double bridged, by the phenol and hydroxide oxygen atoms, giving rise to a Zn_2O_2 metallacycle with Zn···Zn distance of 3.289(1) Å and Zn-O-Zn angles of 95.46(19) and 106.9(2)º. The Zn(II) and Dy(III) ions are triple bridged (through two O_{phenol} and one μ-OH), leading to a short Zn···Dy distance of 3.2009(7) Å and Zn-O-Dy angles close to 90 º. It is noteworthy that the Zn···Dy distance is even shorter than the Zn···Zn one and notably shorter than the shortest one found in $[Zn_2Dy(L')(OAc)_2(NO_3)_2(H_2O)]$ (3.4583(5) Å).

Magnetic Properties

The direct-current (*dc*) magnetic susceptibility studies of all the complexes were performed under a field of 1000 Oe in the temperature range 2–300 K. The plots of $\chi_M T$ *versus* *T* for the mononuclear complexes are shown in Fig. 7 (**2**) and Fig. S2 (**1** and **3**). At room temperature (300 K), the $\chi_M T$ products for **1**, **2** and **3** are 10.35, 14.05 and 12.10 cm^3kmol^{-1}, which are all of them

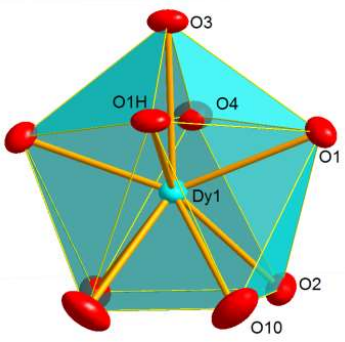

Fig. 6. Coordination environment for Dy in **4**, showing the spherical capped square antiprism structure.

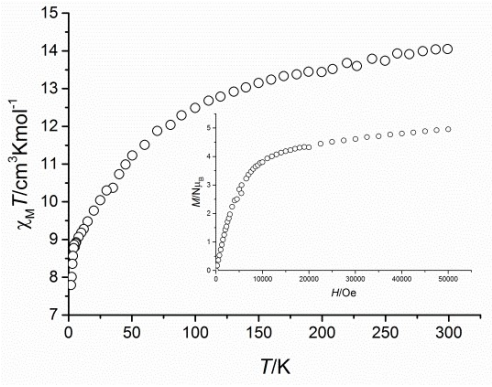

Fig. 7. $\chi_M T$ *vs T* for **2**. Inset: $M/N\mu_B$ *vs H*.

similar to the expected values for uncoupled Tb^{III} ($4f^8$, $^7F_6$), Dy^{III} ($4f^9$, $^6H_{15/2}$) and Er^{III} ($4f^{11}$, $^4I_{15/2}$) ions of 11.82, 14.17 and 11.48 cm^3kmol^{-1}, respectively.

In all cases, the experimental $\chi_M T$ values decrease gradually upon cooling, and more rapidly below 50 K down to minimum values of 5.57, 7.79 and 6.0 cm^3kmol^{-1} at 2 K for **1**, **2** and **3**, respectively. This behaviour seems to be mainly due to the depopulation of the M_J sublevels of the lanthanide ion and maybe to very weak intermolecular interactions, which can be responsible for the more pronounced decrease in $\chi_M T$ at low temperature.

The field dependence of the magnetization at 2 K for the mononuclear **1**, **2** and **3** complexes (Figs 7 and S2) is very similar in all cases and shows a relatively rapid increase of the reduced magnetization at low field without reaching saturation at 5 T. The magnetization value at the maximum applied field of 5 T (in the 4.95–5.32 $Ms/N\mu_B$ range) is significantly lower than the expected one for isolated Tb^{III}, Dy^{III} and Er^{III} ions ($Ms/N\mu_B = g_J J$), which can be attributed to the crystal-field effects that lead to a substantial magnetic anisotropy.

Alternating current (*ac*) magnetic susceptibility measurements were recorded for all these complexes in order to know the low-temperature magnetic relaxation behaviour of the samples. At zero external field, none of the mononuclear compounds show out-of-phase *ac* susceptibilities (χ″) peaks at a frequency of 1200 Hz, as can be seen in Fig. S3. However, it must be noted that, in some cases, the application of a small static magnetic field,[31a] to remove the mixing of the ground ±*Ms* levels, or the dilution of a complex within a diamagnetic matrix, to eliminate dipolar interactions,[32] can partly or fully suppress the quantum tunnelling (QTM) relaxation processes, enabling observation of the slow relaxation process through the real thermally activated energy barrier (*U*). Accordingly, both approximations were tried in order to check the quantum tunnelling effects.

Thus, in an initial approach, the variable temperature *ac* susceptibilities were measured at 1200 Hz with the application of a small *dc* field of 1000 Oe for all the compounds. As shown in Fig. S4, even in these conditions χ_M'' does not reach a maximum above 2 K for none of the mononuclear complexes.

Therefore, in a second attempt to destroy the QTM, *ac* magnetic measurements at 1400 Hz were carried out on a diluted sample of **2@Y** ($[Dy_{0.09}Y_{0.91}(H_3L)(H_2O)(NO_3)](NO_3)_2$), prepared using a Dy/Y 1:10 molar ratio (see experimental). These measurements were recorded both in the absence and in the presence of a *dc* field of 1000 Oe (Fig. S4). No major difference was found in the variation of χ_M'' *vs T* for the diluted **2@Y** sample (Fig. S4) compared to the undiluted **2** one (Fig. S3) and a net peak is not observed even when the diluted sample is subjected to the presence of an external magnetic field.

Accordingly, from the previous experiments it can be concluded that the intermolecular forces and dipolar interactions are insignificant in this case. In view of this, the quantum tunnelling in this complex should be probably due to hyperfine interactions[33-34] but, in any case, none of these mononuclear compounds seem to exhibit slow relaxation of the magnetization, and consequently SMM behaviour.

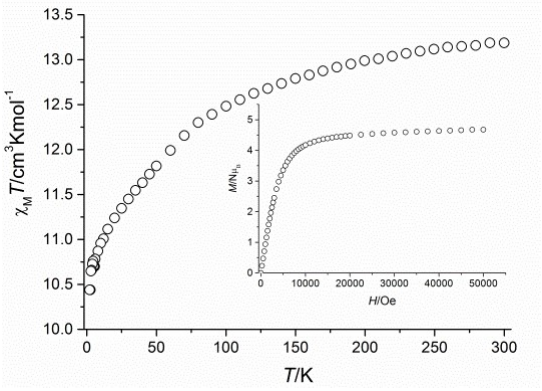

Fig. 8. $\chi_M T$ *vs T* for **4**. Inset: $M/N\mu_B$ *vs H*.

The $\chi_M T$ *versus T* and $M/N\mu_B$ *vs H* graphs for **4** (Fig. 8) also agree with the presence of a non-coupled Dy^{III} ion and the existence of a significant anisotropy.

The potential behaviour of **4** as SMM was also analysed. In this way, *ac* susceptibility measurements were recorded and they demonstrated that **4**·$3H_2O$ does not present out of phase peaks in the absence of an external *dc* field in the 0-20 K range (1200 Hz). Nevertheless, when an optimal *dc* field of 2500 Oe is applied (Fig. S5), χ_M'' shows frequency-dependence and net maxima below 13 K (Fig. 9), indicating that the complex behaves as a field-induced SIM. Besides, it should be noted that Fig. 9 reveals that χ_M'' does not go to zero below the maxima at low temperature, which indicates that the fast relaxation of the magnetization by a QTM mechanism has not been fully suppressed by the application of an optimal external magnetic field.

The Cole-Cole plot for **4** (Fig. S6) between 4 and 12 K affords parameters in the range 0.54-0.22, suggesting multiple relaxation processes. Accordingly, the experimental Arrhenius' plot (Fig. 10)

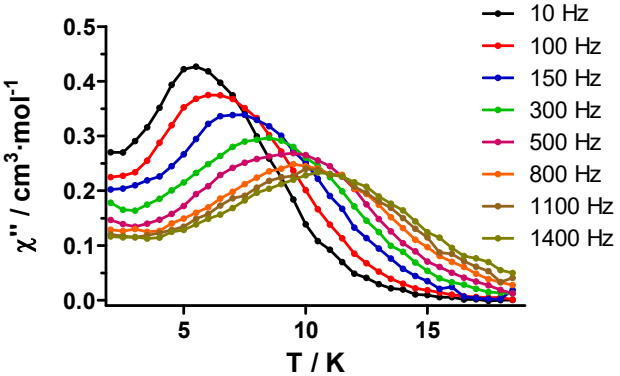

Fig. 9. Temperature dependence of χ_M'' for **4** in a *dc* applied field of 2500 Oe at different frequencies.

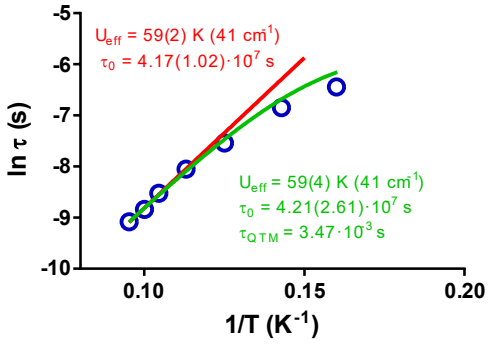

Fig. 10. Arrhenius plot for **4** in a *dc* applied field of 2500 Oe. The red line accounts for the best fit considering Arrhenius relaxation, and the green line corresponds to Orbach plus QTM relaxation (eq. 1).

could not be reproduced just considering Orbach's relaxation but could be satisfactorily fitted to equation 1, which considers contributions from Orbach thermal processes and quantum tunnelling, in agreement with the conclusions extracted from Fig. 9.

$$\tau^{-1} = \tau_{QTM}{}^{-1} + \tau_0{}^{-1}\mathrm{e}^{-U_{eff}/k_B\mathrm{T}} \quad \text{(eq. 1)}$$

The best bit according to equation 1 affords a barrier U_{eff} of 59(4) K, although no hysteresis loop could be observed at 2 K. In spite of this, the U_{eff} value clearly demonstrates that the anisotropy energy barrier in the Zn_2Dy complex **4**·3H$_2$O increases notably respect to the mononuclear Dy sample **2**. One could think that this fact could be related to the small changes in geometry induced by the coordination of the zinc(II) ions. Nevertheless, recent DFT studies[14b] highlight that the coordination number in ZnDy complexes has little influence in the electronic properties. Therefore, other factors must be taken into account. Accordingly, the coordination of Zn(II) to the ligand is accompanied by its full deprotonation, thus probably increasing the charge on the phenol oxygen atoms. In the same way, the water donor in the coordination sphere of the Dy^{3+} ion in **2** has been replaced by a hydroxide donor in **4**·3H$_2$O. All this should leads to a large electrostatic interaction on the dysprosium ion, which, finally, should promote the destabilisation of excited states and therefore an increased ground-state to first excited state gap.[14] However, it has also been demonstrated that the presence of Zn^{II} induces a large charge polarisation on the oxygen atoms that favours an increase in the U_{eff} barrier. In addition, it should be also considered that zinc appears to promote a "dilution effect" of the sample[17] and, therefore, that the presence of Zn seems to favour the SMM behaviour by itself. Accordingly, the increase in the U_{eff} barrier of **4**·3H$_2$O respect to **2** is maybe the result of a series of changes in charge distribution and dilution effects promoted by the presence of zinc.

In addition, when the magnetic properties of **4** are compared with the ones of the related $[Zn_2Dy(L')(OAc)_2(NO_3)_2(H_2O)]$ complex,[30] both with DyO_9 cores, it is observed a net increase in U_{eff} for **4**. Accordingly, in the present complex U_{eff} (59 K) is about 1.2 times the U_{eff} value of the described compound (48 K). Therefore, this comparison makes clear that small changes in the donor groups of the ligand can induce significant changes in the magnetic behaviour and, hence, this work points to the search for new compartmental ligands with different functional groups at the 3-position on the phenolic aromatic ring, which can markedly enhance the anisotropic energy barrier.

Photophysical properties

All spectrophotometric measurements for **1**, **2**, **3** and **4** were taken in methanol solution at 298 K. The photophysical characterisation and the main photophysical data are reported in Table S3. Owing to their similarity, only the absorption and emission spectra of compounds **2** and **4** are depicted (Fig. 11).

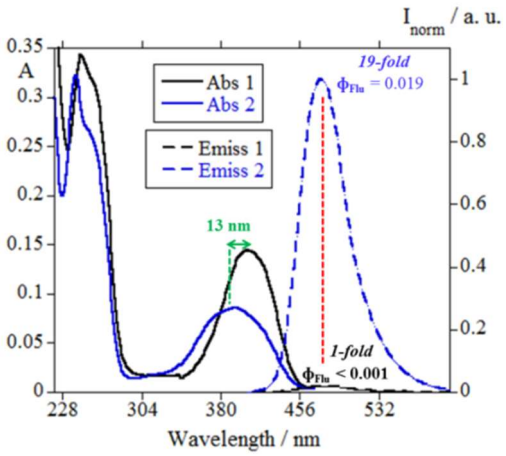

Fig. 11. Absorption and normalised emission spectra of complexes **2** (Abs1 and Emiss1, colour: black), and **4** (Abs2 and Emiss2, colour: blue) in methanol at 298 K (concentration of **2** = **4** = 10^{-5} M, λ_{exc1} = 407, λ_{exc2} = 394 nm, and λ_{em1} = 483, λ_{em2} = 476 nm).

The electronic absorption spectra for dilute solutions of all the metal complexes (10^{-5} M) in methanol show similar features, exemplified in Fig. 11. In this way, three absorption bands are observed at *ca*. 245, 260 and 405 nm, which are attributed to π–π* electronic transitions of the phenol rings and the imine bonds present in all the molecules (see Table S3).[23,35] In all cases, the perfect match between the absorption and the excitation spectra rules out the presence of any emissive impurity, in agreement with the high purity of all the complexes.

As it could be observed in Fig. 11 for **2** and **4**·3H$_2$O, the presence of Zn^{2+} induces a decrease in the absorption band centred at *ca.* 394 nm, what is accompanied by a hypsochromic shift of *ca*. 13 nm. This effect is due to coordination of the imine group to the Zn^{2+} metal ion.

The fluorescence spectra of all compounds display a broad band with a maximum at *ca*. 471-483 nm (Table S3), which seems to be a ligand-based emission, given the broad nature of these signals. In addition, the low fluorescence observed for **1**, **2** and **3** can be ascribed to the absence of coordination between the lanthanide ions and the imine groups of the ligand skeleton. This effect promotes that the Photo-induced Electron Transfer (PET) process takes place from the N_{imine} lone pair to the excited state of the fluorophore (phenol rings).[36] The coordination of metal ions to these nitrogen atoms prevent PET quenching from the lone pair of electrons of each nitrogen atom to the fluorophore moieties. It was reported that d^{10} metal ions (like Zn^{2+}) enhance the fluorescence of this kind of ligand because, usually, these ions do not introduce low-energy metal centred or charge separated excited states into

the molecules, in such a way that the electron-transfer or energy-transfer phenomena cannot commonly occur.[37]

In **4**, the N_{imine} lone pairs are bound to the Zn^{2+} ions preventing the PET process from the imine groups to the adjacent phenol moieties, thus favouring the fluorescence emission.[38] For this reason, complexation with Zn^{2+} results in an enhancement of the fluorescence signal (Chelation Enhanced Fluorescence (CHEF) effect). Thus, a remarkable increase of fluorescence intensity was observed for **4** (19-fold, ϕ_{Flu} = 0.019) compared with **2** (1-fold, ϕ_{Flu} < 0.001), at peak wavelength λ_{max} = 476 nm and λ_{max} = 483 nm, respectively. Accordingly, the presence of Zn in **4**·$3H_2O$ converts it in a dual functional compound, and can be defined as a fluorescent SIM.

Conclusions

New Tb, Dy, Er and Zn2Dy complexes have been obtained from a related api-type compartmental ligand (H_3api = 2-(2-hydroxyphenyl)-1,3-bis[4-(2-hydroxyphenyl)-3-azabut-3-enyl]-1,3-imidazolidine). The isolation and full characterisation of the mononuclear compounds suppose the discovering of a systematic approach for obtaining a new kind of lanthanide-api complex, different from the $[Ln(R\text{-}api)]_2$ sandwich species reported until now as main products of synthetic processes. The characterisation by single X-ray diffraction shows that all the complexes present LnO_9 cores, with structure between muffin-like and spherical capped square antiprism. The full magnetic characterisation reveals that none of the mononuclear complexes behave as SMMs, even when the samples are diluted and a *dc* magnetic field is applied. Nevertheless, heterotrinuclear **4** is a field-induced SIM, with U_{eff} = 59 K, what means that the thermal energy barrier of this Zn_2Dy compound increases significantly respect to the mononuclear **2** one. In addition, the presence of zinc also produces an outstanding increase of the fluorescence in **4** with respect to the mononuclear compounds, in such a way that **4** is a fluorescent SIM. Accordingly, this work demonstrates that the presence of zinc(II) in lanthanide molecular compounds can simultaneously improve their magnetic and luminescent properties and, therefore, their multifuncionality.

Conflicts of interest

There are no conflicts to declare.

Acknowledgements

Authors thank the Spanish Ministerio de Economía y Competitividad (CTQ2014-56312-P), Junta de Andalucía (FQM-195 and Project of excellence P11-FQM-7756), Xunta de Galicia (GRC2015/009) and the University of Granada for financial support. C. Núñez is funded by the Miguel Servet Program (CP16/00139), Instituto de Salud Carlos III, Ministerio de Economía, Industria y Competitividad (Spain).

References

1 See. for example: (a) D. Maspoch, D. Ruiz-Molina and J. Veciana, *Chem. Soc. Rev*., 2007, **36**, 770–818; (b) C. Train, M. Gruselle and M. Verdaguer, Chem. Soc. Rev., 2011, **40**, 3297; (c) Y. Chen and S. Ma, *Rev. Inorg. Chem*., 2012, **32**, 81–100; (d) M. Castellano, R. Ruiz-Garcia, J. Cano, J. Ferrando-Soria, E. Pardo, F. R. Fortea-Perez, S-E. Stiriba, M. Julve and F. Lloret, *Acc. Chem. Res*., 2015, **48**, 510; (e) B. Li, H-M. Wen, Y. Cui, W. Zhou, G. Qian and B. Chen, *Adv. Mat*., 2016, **28**, 8819.

2 J. Rocha, L. D. Carlos, F. A. Almeida Paz and D. Ananias, *Chem. Soc. Rev*., 2011, **40**, 926.

3 K. Mandel, T. Granath, T. Wehner, M. Rey, W. Stracke, N. Vogel, G. Sextl, Gerhard and K. Mueller-Buschbaum, *ACS Nano*, 2017, **11**, 779.

4 (a) H. Gu, R. Zheng, X. Zhang and B. Xu, *J. Am. Chem. Soc.*, 2004, 126, 5664; (b) J.-H. Park, G. von Maltzahn, E. Ruoslahti, S. N. Bhatia and M. J. Sailor, *Angew. Chem. Int. Ed*., 2008, **47**, 7284; (c) K. M. Yeo, C. J. Gao, K.-H. Ahn and I. S. Lee, *Chem. Commun*., 2008, 4622.

5 See for example: (a) C. C. Beedle, C. J. Stephenson, K. J. Heroux, W. Wernsdorfer and D. N. Hendrickson, *Inorg. Chem*., 2008, **47**, 10798; (b) M. Menelaou, F. Ouharrou, L. Rodriguez, O. Roubeau, S. J. Teat, N. Aliaga-Alcalde, *Chem. Eur. J*., 2012, **18**, 11545; (c) S. Mohapatra, B. Raheswaran, A. Chakraborty, A. Sundaresan and T. K. Maji, *Chem. Mater*., 2013, **25**, 1673; (d) M. Ren, S-S. Bao, R. A. S. Ferreira, L-M. Zheng and L. D. Carlos, *Chem. Commun*., 2014, **50**, 7621; (e) Q.-W. Li, J.-L. Liu, J.-H. Jia, Y.-C. Chen, J. Liu, L.-F. Wang and M.-L. Tong, *Chem. Commun*., 2015, **51**, 10291; (f) F. Pointillart, B. Le Guennic, O. Cador, O. Maury and L. Ouahab, *Acc. Chem. Res*., 2015, **48**, 2834; (fg) J-R. Jiménez, I. F. Díaz-Ortega, E. Ruiz, D. Aravena, S. J. A. Pope, E. Colacio and J. M. Herrera, *Chem. Eur. J*., 2016, **22**, 14548; (h) M. Perfetti, F. Pointillart, O. Cador, L. Sorace and L. Ouahab, in *Molecular Magnetic Materials: Concepts and Applications*, First Edition, Wiley-VCH Verlag GmbH & Co. KGaA, 2017, Pg. 345.

6 L. Armelaoa, S. Quici, F. Barigelletti, G. Accorsi, G. Bottaro, M. Cavazzini and E. Tondello, Coord. Chem. Rev., 2010, **254**, 487.

7 D. Zeng, M. Ren, S-S. Bao, L. Li and L-M Zheng, *Chem Commun*., 2014, **50**, 8356.

8 S. Das, K. S. Bejoymohandas, A. Dey, S. Biswas, M. L. P. Reddy, R. Morales, E. Ruiz, S. Titos-Padilla, E. Colacio and V. Chandrasekhar, *Chem. Eur. J*., 2015, **21**, 6449.

9 C. D. Polyzou, C. G. Efthymiou, A. Escuer, L**.** Cunha-Silva, C. Papatriantafyllopoulou and S. P. Perlepes, *Pure App. Chem*., 2013, **85**, 315.

10 S. Osa, T. Kido, N. Matsumoto, N. Re, A. Pochaba and J. A. Mrozinski, *J. Am. Chem. Soc.*, 2004, **126**, 420.

11 L. Piquer and E. C. Sañudo, *Dalton Trans.*, 2015, **44**, 8771.

12 T. Kajiwara, M. Nakano, K. Takahashi and M. Yamashita, *Chem. Eur. J*., 2011, **17**, 196.

13 E. Colacio, J. Ruiz, A. J. Mota, M. A. Palacios, E. Cremades, E. Ruiz, F. J. White and E. K. Brechin, *Inorg. Chem*., 2012, **51**, 5857.

14 (a) A. Upadhyay, S. K. Singh, C. Das, R. Mondol, S. K. Langley, K. S. K. Murray, G. Rajaraman and M. Shanmugam, *Chem. Commun*., 2014, **50**, 8838. (b) A. Upadhyay, C. Das, S. Vaidya, S. K. Singh, T. Gupta, R. Mondol, S. K. Langley, K. S. Murray, G. Rajaraman and M. Shanmugam, *Chem. Eur. J*., 2017, **23**, 4903.

15 A. Watanabe, A. Yamashita, M. Nakano, T. Yamamura and T. Kajiwara, *Chem. Eur. J*., 2011, **17**, 7428.

16 (a) S. Titos-Padilla, J. Ruiz, J. M. Herrera, E. K. Brechin, W. Wersndorfer, F. Lloret and E. Colacio, *Inorg. Chem*., 2013, **52**, 9620. (b) J. P. Costes, S. Titos-Padilla, I. Oyarzabal, T. Gupta, C. Duhayon, G. Rajaraman and E. Colacio, *Chem. Eur. J*., 2015, **21**,

15785. (d) J. P. Costes, S. Titos-Padilla, I. Oyarzabal, T. Gupta, C. Duhayon, G. Rajaraman and E. Colacio, *Inorg. Chem.*, 2016, **55**, 4428.
17 A. Amjad, A. M. Madalan, M. Andruh, A. Caneschi, L. Sorace, *Chem. Eur. J.*, 2016, **22**, 12849.
18 M. Fondo, A. M. García-Deibe, N. Ocampo, J. Sanmartín and M. R. Bermejo, *Polyhedron*, 2008, **27**, 2585.
19 *SADABS: Area-Detector Absorption Correction*. Siemens Industrial Automation, Inc.: Madison, WI, 1996.
20 *SHELX Programs for Crystal Structure Analysis*. G. M. Sheldrick, Institüt für Anorganische Chemie der Universität, Göttingen, *Acta Crystallogr. A*, 2008, **64,** 112.
21 (a) S. R. Meech and D. *J.* Philips, *Photochem*., 1983, **23**, 193. (b) M. Montalti, A. Credi, L. Prodi and M. T. Gandolfi, *Handbook of Photochemistry*, 3rd ed.; CRC, Taylor & Francis Group: Boca Raton, New York, NY, 2006.
22 L. W. Yang, S. Liu, E. Wong, S. J. Retting and C. Orvig, *Inorg. Chem.*, 1995, **34**, 2164.
23 R. C. Howell, K. V. N. Spence, I. A. Kahwa and D. J. Williams, *J. Chem. Soc., Dalton Trans*., 1998, 2727.
24 J. Chakraborty, S. Thakurta, G. Pilet, R. F. Ziessel, L. J. Charbonnière and S. Mitra, *Eur. J. Inorg. Chem*., 2009, 3993.
25 M. Nematirad, W. J. Gee, S. K. Langley, N. F. Chilton, B. Moubaraki, K. S. Murray and S. R. Batten, *Dalton Trans*., 2012, **41**, 13711.
26 L. Zhao, J. Wu, H. Ke and J. Tang, *CrystEngComm*, 2013, **15**, 5301.
27 I. A. Kahwa, F. R. Fronczek and J. Selbin, *Inorg. Chim. Acta*, 1988, **148**, 273.
28 K. Nakamoto, *Infrared and Raman Spectra of Inorganic and Coordination Compounds*, Ed. John Wiley & Sons, New York, 1997.
29 (a) M. Llunell, D. Casanova, J. Cirera, J. M. Bofill, P. Alemany, S. Alvarez, M. Pinsky and D. Avnir, *D. SHAPE v1.1b*, Barcelona, 2005; (b) A. Ruiz-Martínez, D. Casanova and S. Alvarez, *Chem. Eur. J.*, 2008, **14**, 1291; (c) M. Llunell, D. Casanova, J. Cirera, P. Alemany and S. Alvarez, SHAPE: *Program for the stereochemical analysis of molecular fragments by means of continuous shape measures and associated tools*, University of Barcelona, Barcelona, Spain, 2010.
30 M. Fondo, J. Corredoira-Vázquez, A. M. García-Deibe, J. Sanmartín-Matalobos, J. M. Herrera and E. Colacio, *Inorg. Chem.*, 2017, **56**, 5646.
31 (a) J. Ruiz, A. J. Mota, A. Rodríguez-Diéguez, S. Titos, J. M. Herrera, E. Ruiz, E. Cremades, J. P. Costes and E. Colacio, *Chem. Commun*., 2012, **48**, 7916; (b) A. Zabala-Lekuona, J. Cepeda, I. Oyarzabal, A. Rodriguez-Dieguez, J. A. Garcia, J. M. Seco and E. Colacio, *CrystEngComm*, 2017, **19**, 256.
32 K. R. Meihaus, J. D Rinehart and J. R. Long, *Inorg. Chem*. 2011, **50**, 8484.
33 F. Luis, M. J. Martínez-Pérez, O. Montero, E. Coronado, S. Cardona-Serra, C. Martí-Gastaldo, J. M. Clemente-Juan, J. Sesé, D. Drung, and T. Schurig, *Phys. Rev. B*, 2010 **82**, 060403.
34 (a) F. Pointillart, K. Bernot, S. Golhen, B. Le Guennic, T. Guizouarn, L. Ouahab, O. Cador, *Angew. Chem., Int. Ed*., 2015, **54**, 1504. (b) Y. Kishi, F. Pointillart, B. Lefeuvre, F. Riobé, B. Le Guennic, S. Golhen, O. Cador, O. Maury, H. Fujiwara and L. Ouahab, *Chem. Commun.*, 2017, **53**, 3575.
35 (a) E. Pretsch, T. Clerc, J. Seibl and W. Simon, *Tables of spectral sata for structure determination of organic compounds*, Springer-Verlag, Berlin, 2nd edn., 1989. (b) M. Fondo, A. M. García-Deibe, N. Ocampo, J. Sanmartín, M. R. Bermejo, E. Oliveira and C. Lodeiro, *New J. Chem*., 2008, **32**, 247.
36 (a) M. T. Albelda, P. Díaz, E. García-España, J. C. Lima, C. Lodeiro, J. Seixas de Melo, A. J. Parola, F. Pina and C. Soriano, *Chem. Phys. Lett.*, 2002, **353**, 63. (b) J. Seixas de Melo, J. Pina, F. Pina, C. Lodeiro, A. J. Parola, J.C. Lima, M. T. Albelda, M. P. Clares, E. García-España and C. J. Soriano, *Phys. Chem. A*, 2003, **107**, 11307.
37 A. Tamayo, B. Pedras, C. Lodeiro, L. Escriche, J. Casabó, J. L. Capelo, B. Covelo, R. Kivekäs and R. Sillanpää, *Inorg. Chem.*, 2007, **46**, 7818.
38 C. Núñez, E. Oliveira, L. Giestas, L. Valencia, A. Macías, J. C. Lima, R. Bastida and C. Lodeiro, *Inorg. Chim. Acta*, 2008, **361**, 2183.